Flow Control of Jet Flow by Passive Nozzle Configuration Changes

Shakouchi, T., Kito, M., Sakamoto, T., Tsujimoto, K. and Ando, T.
Graduate School of Engineering, Mie University
Kurimamachiya-cho 1577, Tsu-shi, Mie 514-8507, Japan
Phone, fax: +81-059-231-9384
shako@mach.mie-u.ac.jp

ABSTRACT

Nozzle configuration may offer the possibility of a passive control technique to provide high mixing and heat transfer rates. Thus, numbers of investigations have been carried out to reveal the influence of nozzle configuration on the flow characteristics. However, very few papers in the scientific literature have focused on orifice jets. Despite the evidence indicating that orifice jets improve the mixing and heat transfer characteristics, we were unable to find a systematic study of them that focused on the contraction area ratio. The effects of varying the contraction area ratio *CR* from 1.00 to 0.11 on the flow characteristics of a free jet issuing from an orifice nozzle were examined. The large vortex structure of a submerged orifice water jet was visualized by the tracer method, which indicated the coherent vortex structure was highly affected by the *CR* value. The mean and fluctuating velocities of the orifice air jet were also measured using a single hot-wire and the effects of *CR* on them were demonstrated. It is found that the normalized centerline maximum velocity could be expressed by $u_c/u_m = 1.9CR^3 - 3.55CR^2 + 1.38CR + 1.53$, showing a maximum value of 1.7 at $CR = 0.27$. In addition, the high spreading and entrainment rates were obtained for smaller value of *CR* indicating that the potential of an effective passive control technique.

Key Words: Jet, Circular Orifice, Contraction Effects, Velocity Distribution, Turbulent Flow, Flow Visualization

1. INTRODUCTION

The application of impinging jets for cooling, drying, and cleaning can be found in a wide variety of industries by virtue of their high heat and mass transfer on and around the stagnation point. It is therefore a challenging subject for many researchers in both the academic and industrial fields. Viskanta [1] provided detailed reviews of impingement heat transfer. Since the understanding of free jets is essential to reveal the mechanism of impinging jets and improve technical methods, the effects of nozzle configurations, jet velocity, and ambient conditions have been well recognized. The nozzle configurations include asymmetric, two-dimensional, and three-dimensional (non-circular) nozzles. Antonia and Zhao [2] examined two circular jets: a pipe jet with a fully developed turbulent flow profile and a contraction jet with a laminar top-hat velocity profile at the nozzle exit.

Although orifice jets are well known for their interesting character - vena contracta effect - and having the high performance of mixing and heat transfer characteristics, little on the subject may be found. Lee and Lee [3] used three different orifice nozzles, namely, squared-, standard-, and sharp-edged, and demonstrated that the edge configuration of orifice nozzles affects the heat transfer characteristics of jet impingement significantly in the stagnation region. They found that the sharp-edged orifice jet enhanced heat transfer rates most among the three orifice nozzles because it provided thin shear layer at the nozzle exit. They referred to the possibility of the nozzle configuration for an effective passive control technique. Quinn [4] also demonstrated the effects of nozzle configurations on the mixing characteristics from mean velocity and pressure distributions of an orifice plate and contoured nozzle jets. The measurement results described stronger mixing characteristics for the jet through the orifice plate. Mi *et al*. [5] investigated the mixing characteristics and physical mechanisms of jets issuing from an orifice plate using flow visualization images and temperature in comparison with a contoured nozzle and a pipe and found that the mixing rate of the orifice plate jet was higher than the

others mentioning the poor understanding the effects of nozzle configuration on the flow characteristics.

Despite the evidence indicating that orifice jets improve the mixing and heat transfer characteristics, we were unable to find a systematic study of them that focused on the contraction area ratio. This paper reveals the effects of the orifice contraction area ratio experimentally by means of flow visualization images and hot- wire measurements.

2. NOZZLE CONFIGURATION AND MEASUREMENT TECHNIQUES

The nozzle configuration is presented in Fig. 1. To evaluate the effect of the contraction area ratio $CR = A_0/A_i$ (A_0: cross sectional area of nozzle exit, A_i: cross sectional area of pipe) of an orifice nozzle on free jet flow characteristics, four different orifice nozzles with CR = 0.69, 0.44, 0.27, and 0.11 corresponding to pipe diameter d_i = 12.00, 15.00, 19.23, and 29.75 mm, respectively, were designed as summarized in Table 1. A pipe nozzle having a fully developed turbulent pipe flow exit velocity profile was also utilized. The pipe corresponding to CR = 1.00 had a 10.0-mm-exit diameter. Every nozzle had an exit diameter d_0 = 10.0 mm, thickness of 1.0 mm and length of 500 mm to ensure a fully developed turbulent pipe flow at the nozzle exit. Note that all the jets issued from a pipe having an exit velocity profile matching that of a fully developed turbulent pipe flow even in the case of a pipe with the diameter d_i = 29.75 mm, for which the pipe length ratio L/d_i = 16.8. A quadrant nozzle providing a uniform velocity profile at the nozzle exit, which can be regarded as the standard profile for fundamental numerical and experimental study, was also used for comparison with the orifice nozzles. The quadrant nozzle contracted from a diameter of 29.75 mm to the exit diameter of 10.0 mm, which smoothly connected to a 3.0-mm-long straight contour.

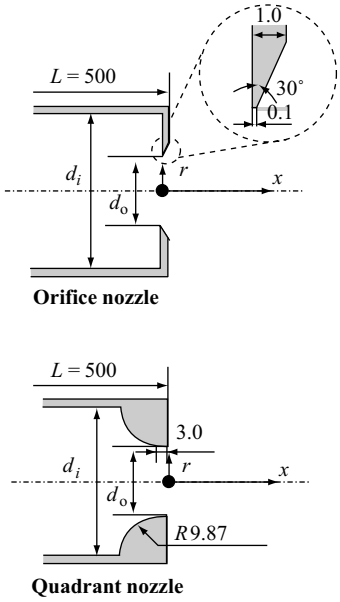

Figure 1. Nozzle and coordinate system (All dimensions in mm).

Table 1. Nozzle specifications

Nozzle type	Contraction ratio $CR = (d_o/d_i)^2$	Pipe inner diameter d_i	Exit diameter d_o
Pipe	1.00	10.0	10.0
Orifice	0.69	12.0	
	0.44	15.0	
	0.27	19.23	
	0.11	29.75	
Quadrant	0.11	29.75	

The x and r axes starting at the origin of the jet were taken in the streamwise and spanwise directions, respectively. In the cross stream direction, the origin $r = 0$ was taken at the centerline of the jet.

A constant temperature hot-wire anemometer was used to measure the mean and fluctuating velocity for an air jet Reynolds number, based on the nozzle exit diameter and jet exit velocity, ranging from 3000 to 15,000. The hot-wire was a single 5-μm I-probe made of tungsten with a sensing length 0.8 mm and prong spacing of 2 mm. The total sampling number was more than 100,000, which should be sufficient to ensure an analysis of higher-order moments.

For low Reynolds number cases (Re = 1000-3000), flow visualisation was performed in a sufficiently large water tank. Water jets seeded homogenously with Uranine (fluorescein) issued from the nozzle into the water tank. The images of vortex structures were recorded with a digital video camera by illuminating the flow in the middle plane.

3. RESULTS AND DISCUSSION

3.1. Nozzle Exit Conditions

The mean exit velocity profiles at Re = 15,000 are plotted on the left side of Fig. 2 and the fluctuating velocity on the right side for each CR because of axisymmetry. The mean velocity profile of CR = 1.00 matched a fully developed turbulent pipe flow. On the other hand, the CR had a considerable effect on the exit velocity profile. In the case of CR = 0.69, the profile was nearly a top-hat and a stronger effect of contraction was observed as CR decreased. The orifice jets had saddle-shaped profiles due to the vena contracta effect and the smaller CR had a thinner shear layer. The exit velocity of a quadrant nozzle also had a thin shear layer. However, the flow distributed uniformly over the nozzle exit was wider than the orifice jets because there was no vena contracta effect. It is therefore not surprising that the quadrant jet velocity u_c/u_m was smaller than the others. The orifice jet velocity at the centre was $u_c/u_m \cong 1.3$ for all the orifices. The smaller CR caused a smaller orifice jet width, reflecting the maximum velocity value. The maximum fluctuating velocities are observed at the largest velocity gradients. The value of the turbulent intensity at the jet centre decreased from 4.3% to 0.2% with decreasing CR.

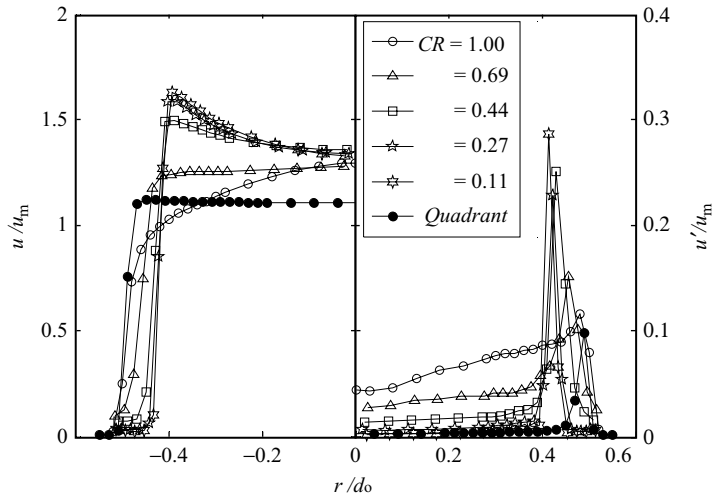

Figure 2. Mean and fluctuating velocity at nozzle exit (x/d_o = 0.2).

3.2. Flow Visualizations

The vortex structures of the submerged orifice water jet were visualized by the tracer method and the effects of CR on them were examined. The results in the middle plane are shown in Fig. 3 for different CR values at Re = 1000 and 3000. Figure 3 clearly shows CR dependency on the jet width at the nozzle exit. The orifice nozzle of CR=0.11 yielded the narrow jet width at the nozzle exit due to the strong contraction. All of the flows were initially laminar and eventually became turbulent following the transition process.

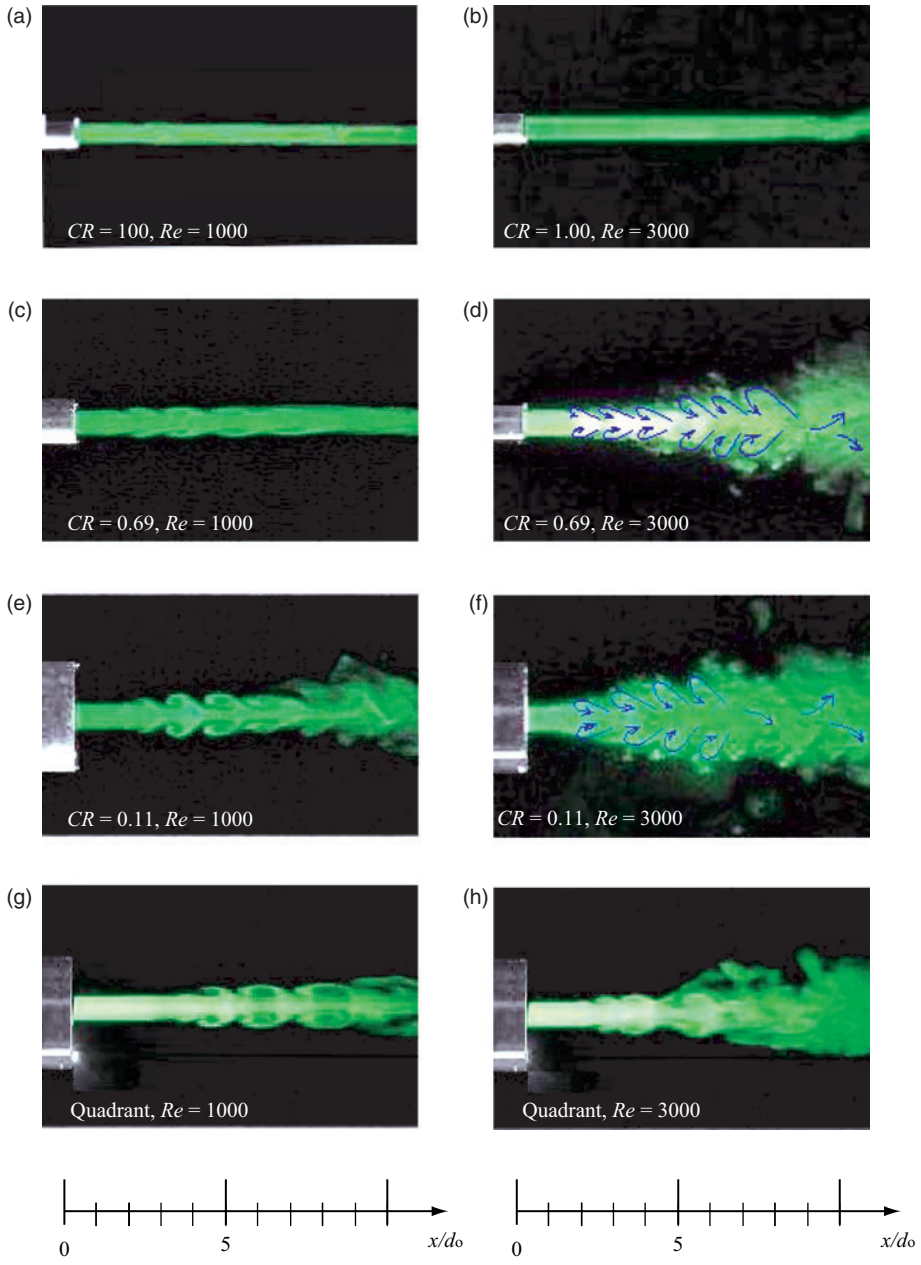

Figure 3. Visualized flow pattern.

There is no clear vortex in the pipe flow in Fig. 3(a), even at $Re = 3000$, except at the very downstream in Fig. 3(b). In contrast, outstandingly large coherent vortexes were observed in Figs. 3(c)-(h). Although it was not so clear at $Re = 3000$, the large vortex structure of the orifice jets could be observed as accentuated with arrow lines showing the flow direction roughly. Detailed observations of movies of the orifices jets revealed the production process of the large vortexes. At first, many vortex rings were produced at the exit of the nozzle due to instability at the edge. A rapid decay in velocity downstream prevented the vortex rings, which yielded a large vortex structure. The contraction ratio CR causes significant changed in the formation of vortices. These changes must be related to the development of shear layer instability at the exit. The vortex rings in Fig. 3(c) are not as clear as those in Fig. 3(e). The coherent vortex rings in Fig. 3(c) seem too week to affect the flow inside the jet, while those in Fig. 3(e) are large enough to affect the core of the jet and retard the flow. The flow issuing from $CR = 0.11$ spread wider and mixed with the ambient fluid faster in the downstream region than that from $CR = 0.69$. The mean velocity for $CR = 0.11$ grew higher and decayed more quickly than that for $CR = 0.69$, as explained in the next section. This may be the reason

for the difference in the vortex size. Coherent vortex yields high mixing and heat transfer rates. Therefore, changing orifice nozzle contraction ratio would offer the better performance in flow and heat transfer characteristics by controlling the coherent structure. Figure 3(g) also shows clear coherent vortexes produced by a quadrant nozzle due to instability at the edge of the nozzle exit, reflecting the thin shear layer as shown in Fig. 2. The large vortexes were stretched and appeared in the downstream region compared with the jet from the orifice nozzle having the same contraction area ratio $CR = 0.11$ in Fig. 3(e). It should also be mentioned that the jet from the quadrant nozzle did not grow as wide as those from the orifice nozzles. The flow from $CR = 0.11$ apparently spread wider and faster than the others. Therefore, the visualized images demonstrated that the smaller CR enhanced the mixing rate more.

3.3. Centerline Measurements at Low Reynolds Number

Figures 4(a) and (b) present centerline velocity u_c/u_m and turbulent intensity u'_c/u_m, respectively, for air jets from the pipe at Reynolds numbers ranging from 3000 to 10,000, which shows the Reynolds number dependency. The potential core in which the jet velocity remained nearly constant from the nozzle exit existed up to $x/d_o = 9$, 7, and 3 for $Re = 3000$, 5000, and 7000, respectively. The centerline velocity then decayed more rapidly at lower Re due to the increase in the turbulent intensity and could be fitted with Eq. (1) in the fully developed region.

$$u_c/u_m \propto (x/d_o)^a \tag{1}$$

where a = –1.96, –1.38, –1.16, and –1.0 for $Re = 3000$, 5000, 7000, and 10,000, respectively.

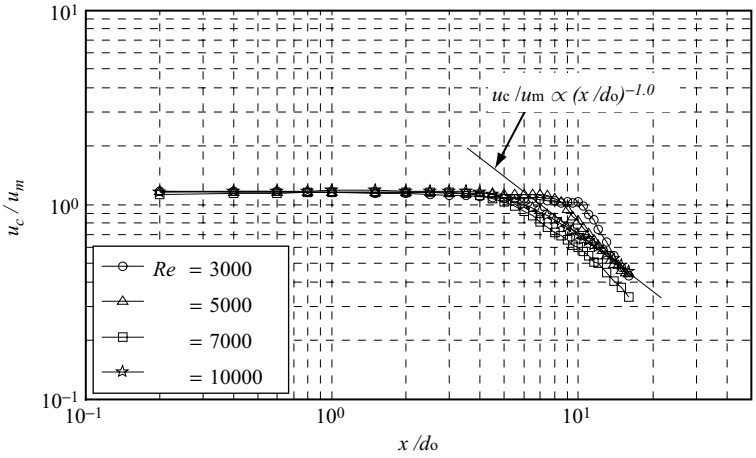

(a) Centerline velocity

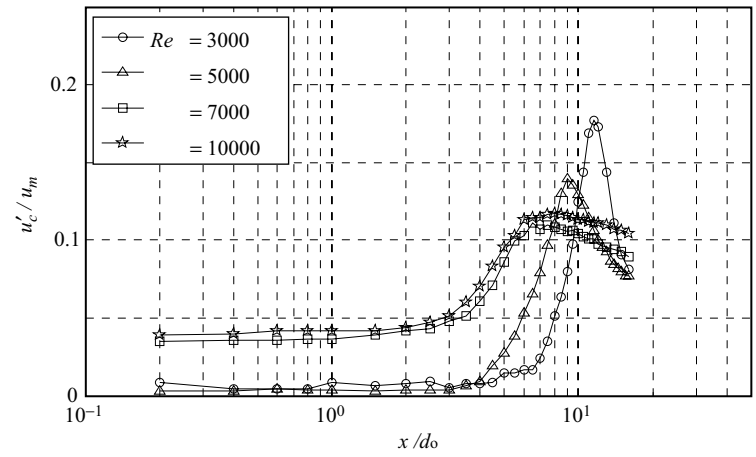

(b) Centerline turbulent intensity

Figure 4. Pipe nozzle ($CR = 1.00$).

At Re = 3000 and 5000, the transition region which is in between the potential core and the fully developed regions was hardly seen, but at $Re \geqq 7000$, it exited in $4 < x/d_o < 8$.

There was only one peak in the turbulent intensity distribution over the whole Reynolds number range, which approached the nozzle exit as Re increased, corresponding to the length of the potential core. It should be mentioned that measurements of u'_c/u_m at higher Reynolds number were initially much larger than those of at lower Re, but its peak decreased with increasing Re. The accuracy of the velocity measurements ranged from 3% to 2% with respect to the maximum value. Examples of orifice jets measurements for CR = 0.11 are shown in Fig. 5. The exit velocity vector towards the centre due to the strong contraction of the orifice nozzle accelerated the centerline velocity from the nozzle exit. After increasing, the centerline velocity remained nearly constant and then decayed. This decay in the fully developed region is well expressed by Eq. (1) with a different constant, but settled to a = -1.0 for high Re. It should be emphasized that the centerline turbulent intensity distribution for orifice jets had two peaks, which did not appear in the case of the pipe jets. The first peak, which appeared at $x/d_o \cong$ 2-4, could be attributed to the turbulent increase resulting from large vortices, as seen in the water jet images. The sudden increase in turbulence for orifice jets occurred earlier, at $x/d_o \cong 1$, than that for the pipe jets. It is also worth noting that the centerline turbulent intensity distribution with one peak was obtained for CR = 0.69 at Re = 3000. This indicates a small effect of vortices produced by the orifice nozzle on the centerline flow showing the same behavior as a pipe flow.

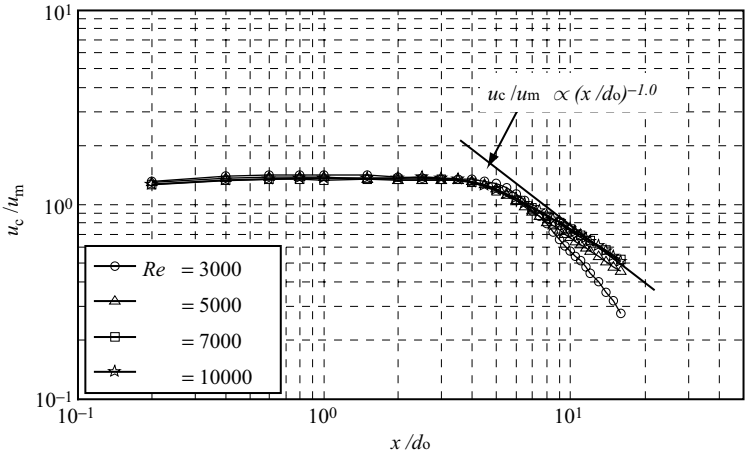

(a) Centerline velocity

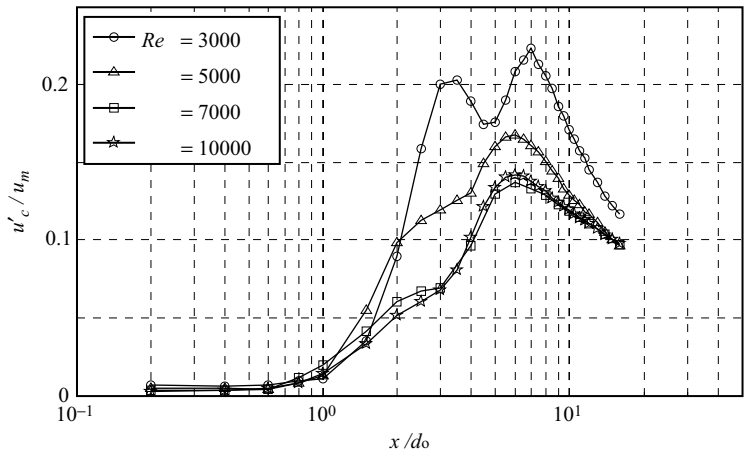

(b) Centerline turbulent intensity

Figure 5. Orifice nozzle (CR = 0.11).

Centerline measurements for the quadrant jet are presented in Fig. 6. The centerline velocity remained nearly constant, as previously mentioned for the pipe jet case, and decayed with $u_c/u_m \propto (x/d_o)^{-1.0}$ at Re = 10,000. It was however unique that the transition region could hardly exist even at high Reynolds number, which indicates that the jet spread suddenly after experiencing the potential core region. The two peaks also appeared in the turbulent intensity distribution corresponding to the large coherent vortexes exhibited in the visualized images.

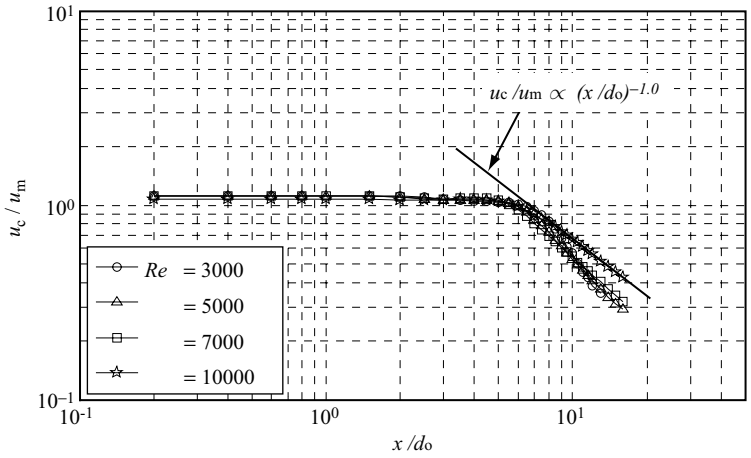

(a) Centerline velocity

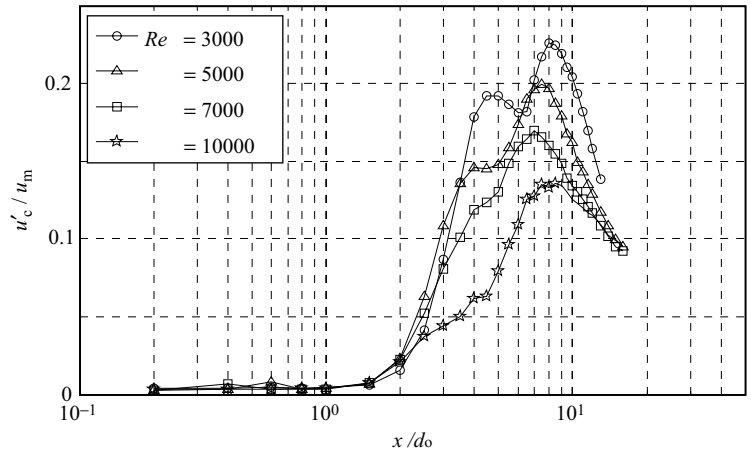

(b) Centerline turbulent intensity

Figure 6. Quadrant nozzle.

3.4. Centerline Measurements at *Re* = 15,000

The flow characteristics at low Reynolds number were investigated by means of submerged water jets visualized images and air jet hot-wire measurements. For more practical use, here we present the detailed air flow characteristics at Re = 15,000, which should be sufficiently higher to describe incompressible flow.

Centerline velocity u_c/u_m and turbulent intensity u'_c/u_m for various CR values with a quadrant nozzle at Re = 15,000 are shown in Figs. 7(a) and (b). The centerline velocity increased from the nozzle exit and reached to the maximum at x/d_o=2.0 for all of the orifice nozzles due to vena contracta effect, while the velocity kept almost constant from the nozzle exit up to $x/d_o \cong 4.0$ and 5.0 for the jets from CR = 1.00 (pipe nozzle) and the quadrant nozzle, respectively. Thereafter the velocity decayed with $u_c/u_m \propto (x/d_o)^{-1.0}$ in the fully developed region. The velocity growth from the exit increased with decreasing CR.

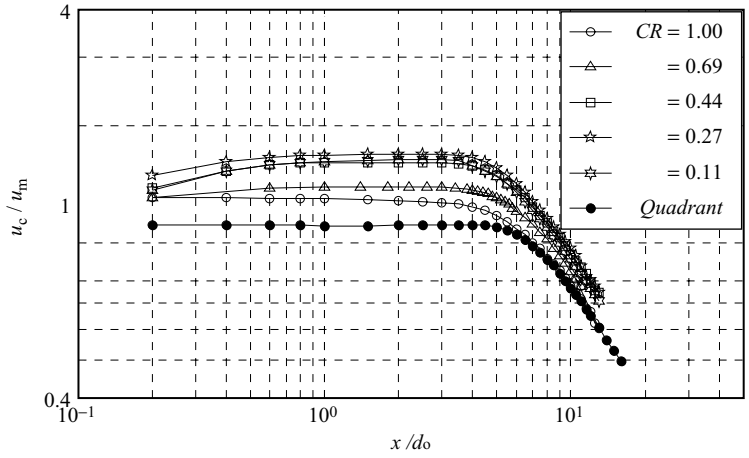

(a) Centerline velocity

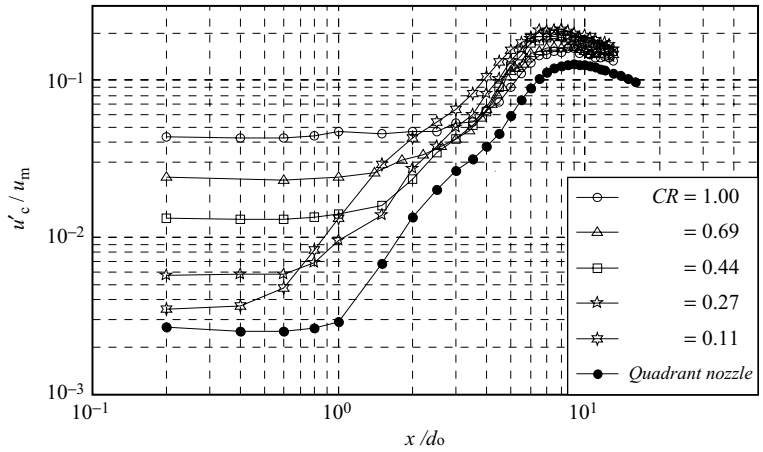

(b) Centerline turbulent intensity

Figure 7. Centerline mean and fluctuating velocities at $Re = 15000$.

The obtained turbulent intensity was apparently smaller at the exit and increased earlier for smaller CR. In the case of $CR = 0.11$, for instance, the sudden increase in turbulent intensity occurred at $x/d_o \cong 0.4$ and the maximum was at $x/d_o \cong 7.0$.

The centerline maximum velocities for different value of CR at $x/d_o = 2.0$ are summarized in Fig 8. The centerline maximum velocity u_c/u_m can be expressed

$$u_c / u_m = 1.9CR^3 - 3.55CR^2 + 1.38CR + 1.53 \quad (2)$$

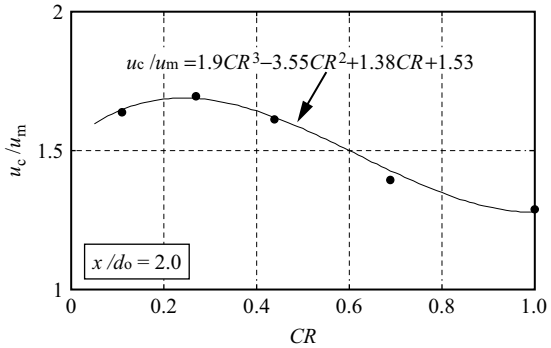

Figure 8. Centerline maximum velocity ($x / d_o = 2.0$).

which has a maximum value of 1.7 at $CR = 0.27$. Velocity vectors towards the centerline produced by strong contraction at the orifice nozzle exit contributed to the increase in the centerline velocity, which had the maximum of $CR = 0.27$.

In order to obtain the dominant frequency of jet fluctuation where the jet reached its maximum velocity at $x/d_o = 2.0$, the power spectra were calculated from the velocity fluctuations at the jet center, as plotted in Fig. 9. The power spectra were normalized integrating the function Φ_u^* as follows: $\int \Phi_u^*(f^*)df^* = 1$, proposed by Mi *et al.* [5] for a comparison. The peak frequencies obtained for $CR = 1.00$ (pipe nozzle), 0.27, 0.69, 0.11, and quadrant nozzle were $f^* = 0.39$, 0.48, 0.55, 0.71, and 0.39, respectively, although the peak was not clear for $CR = 1.00$ (pipe nozzle). The values for the quadrant nozzle and $CR = 0.11$ are consistent with those reported by Mi *et al.* [5]. They presented that $f^* \approx 0.40$ for a contoured nozzle and $f^* \approx 0.70$ for an orifice. Clearly, the peak frequency decreases with increasing CR. In addition, the magnitude Φ_u^* at the peak decreases as well and the peak becomes obscure, reflecting large coherent vortex disintegrations. Those results, suggest that the same coherent vortex structures seen in Fig. 3 at low Re, might exist at high Re as well.

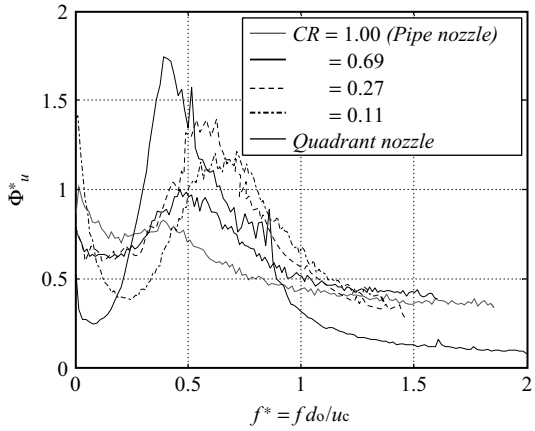

Figure 9. Power spectra at $x/d_o = 2.0$.

The skewness and flatness variations along the centerline are shown in Fig. 10. Decreasing skewness implies the domination of low-velocity components. The gradient of the decreasing skewness for the orifice jets and quadrant jet was steeper than that of the pipe jet. This might be related to the shear layer thickness. The minimum peaks of the skewness occurred at $x/d_o = 4$, 4.5, and 5 for orifice jets, the pipe jet, and the quadrant jet, respectively. The minimum peaks seem to be consistent with each potential core length and the flatness values were more than 3, which implies the existence of the intermittent

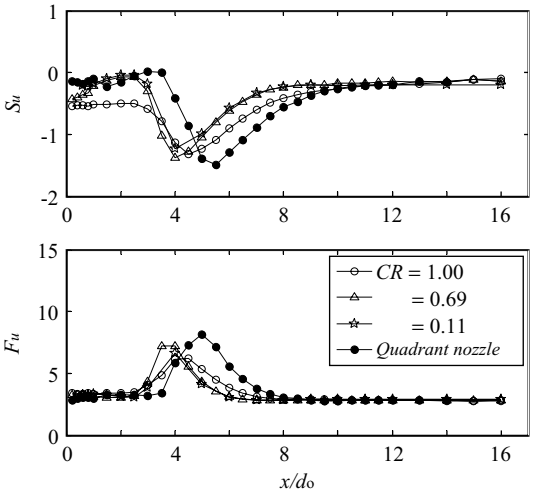

Figure 10. Variation of skewness and flatness factors along the centerline.

vortexes explained by Gad-el-Hak and Brandyopadhyay [6] and Simpson *et al*. [7]. In orifice jets, the regions with dominant low-velocity components were smaller and the flow started to shed the low-velocity components into the outer layer faster than the other jets. The developing region could be associated with the region from the location at the minimum skewness to where the skewness exhibited constant behavior. The region in orifice jets were shorter than in the other jets, indicating that the orifice jets grew faster than the others and had a high entrainment flow rate. Downstream, the skewness and flatness factors approached Gaussian characteristics, i.e. $S_u = 0$, $F_u = 3$, for all of the jets.

3.5. Spreading of the Jet

The cross sectional mean and fluctuating velocity at $Re = 15{,}000$ are shown in Fig. 11. Even though the effects of vena contracta were moderated at $x/d_o = 1.0$, the maximum velocity at the jet center was higher than for the pipe jet with a fully developed turbulent pipe flow at the nozzle exit. A steeper velocity gradient was observed at the edge of the jet for a smaller *CR* producing higher turbulence due to the strong shear force. In addition, we found that every cross sectional velocity profile matched to the Tollmien's theoretical solution at $x/d_o > 5.0$.

Therefore, the exit velocity profile had negligible impact on the distance from the nozzle exit to the fully developed region.

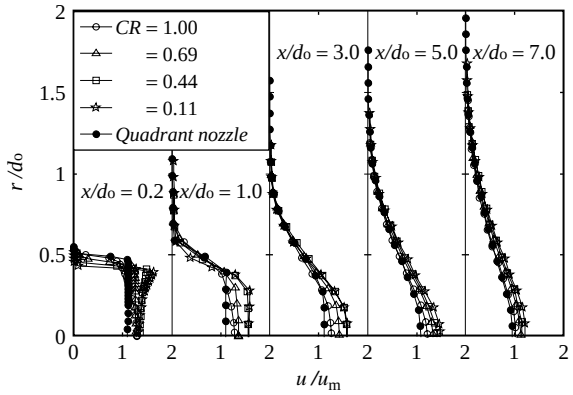

(a) Mean velocity

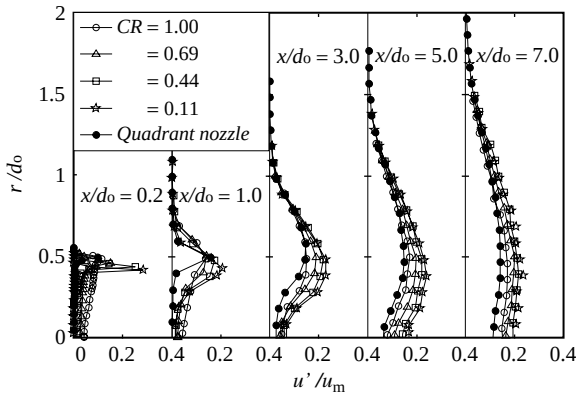

(b) Turbulent intensity

Figure 11. Mean and fluctuating velocity.

The jet and half widths are plotted in Fig. 12. The jet width was determined from the location where the velocity ratio $u/u_c = 0.1$. Both widths varied with *CR* at $x/d_o < 5$. A larger *CR* provided larger widths corresponding to the shear layer thickness. However, the jets for a smaller *CR* grew so fast that both widths in all the cases matched at $x/d_o > 5$. This rapid growth poses the increase in entrainment flow rate. In addition, the half jet width can be expressed by the following:

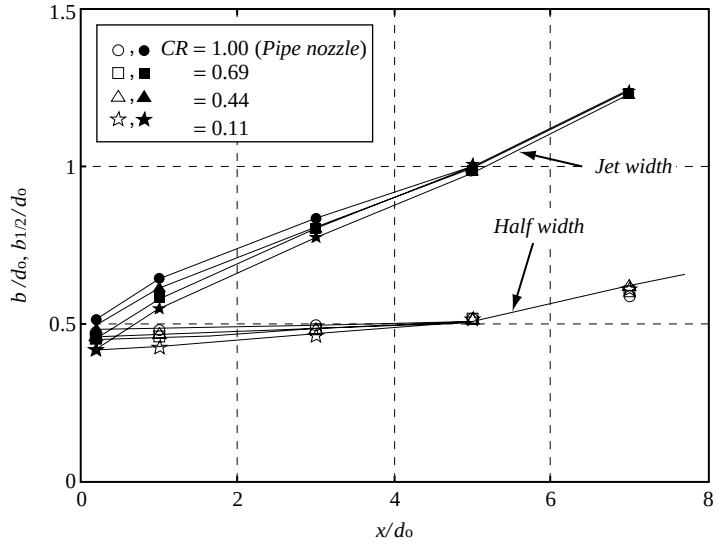

Figure 12. Jet and half widths.

· $2 < x/d_o < 5$

$$
\begin{aligned}
b_{1/2}/d_o &= 0.006\,(x/d_o) + 0.481 \quad \text{for} \quad CR = 1.00 \\
&= 0.012\,(x/d_o) + 0.458 \quad \text{for} \quad = 0.69 \\
&= 0.017\,(x/d_o) + 0.431 \quad \text{for} \quad = 0.44 \\
&= 0.019\,(x/d_o) + 0.414 \quad \text{for} \quad = 0.11
\end{aligned}
\tag{3}
$$

· $5 < x/d_o$

$$
b_{1/2}/d_o = 0.048\,(x/d_o) + 0.273 \quad \text{for} \quad CR = 1.00\text{-}0.11 \tag{4}
$$

The measured ratios of entrainment flow rate to the exit flow rate are plotted in Fig. 13 along with the equation given by Boguslawski and Popiel [8] for pipe jet data. The flow rate at location x, Q_x, was determined by $Q_x = 2\pi \int_0^{\delta} urdr$, where δ is the radial location at $u/u_m = 0.01$ and Q_0 is the flow rate at the nozzle exit. Satisfactory agreement could be observed between the present pipe jet data and the line in the form of $[(Q_x - Q_0)/Q_0] = 0.183(x/d_o)$ suggested by Boguslawski and Popiel [8]. In the case of the quadrant jet, the entrainment growth seemed slightly different from the pipe jet and was found to be expressed by $[(Q_x - Q_0)/Q_0] = 0.201(x/d_o)$. A sudden increase in the entrainment flow rate due to the thin shear layer, as shown in Fig. 2, whose instability promoted the entrainment of the ambient fluid, was observed in the near field $x/d_o<1$. Then, the entrainment flow rate increased linearly from $x/d_o>3$ with decreasing *CR*. This relationship in terms of the non-dimensional distance from the exit may be expressed from the present data by the following:

· $3 < x/d_o$

$$
\begin{aligned}
[(Q_x - Q_0)/Q_0] &= 0.204(x/d_o) \quad \text{for} \quad CR = 0.69 \\
&= 0.227(x/d_o) \quad \text{for} \quad CR = 0.44 \\
&= 0.251(x/d_o) \quad \text{for} \quad CR = 0.27 \\
&= 0.271(x/d_o) \quad \text{for} \quad CR = 0.11
\end{aligned}
\tag{5}
$$

These results indicate that *CR* affected the entrainment rate, making the jets from the smaller *CR* entrain ambient fluid more in the far field $x/d_o > 3$.

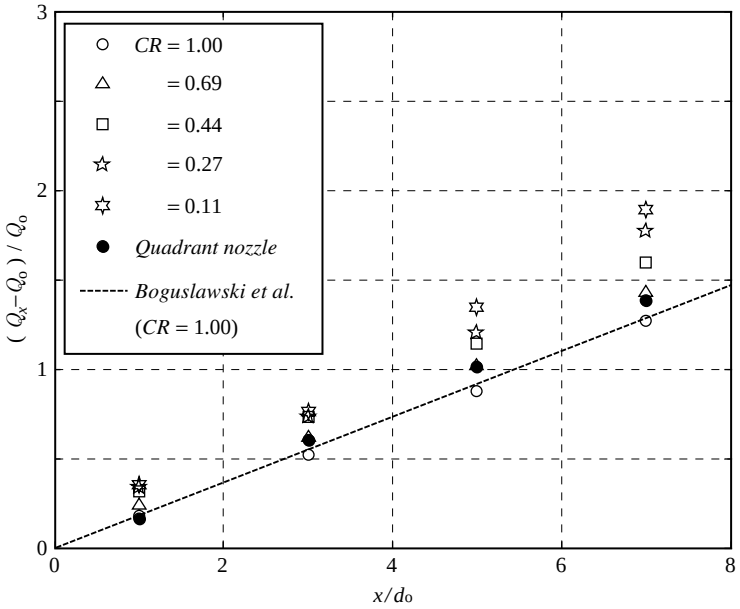

Figure 13. Entrainment flow rate ratio.

3.6. Pressure Drop

Figure 14 shows the relation between the pressure drop, Δp, and CR. The Δp is the pressure difference between atmospheric pressure and the static pressure on the pipe wall at $20d_o$ upstream from the nozzle exit. The pressure drop increased with decreasing CR. The smaller CR, however, increased the centerline velocity because of the strong vena contracta effects, as it was mentioned in Fig. 7.

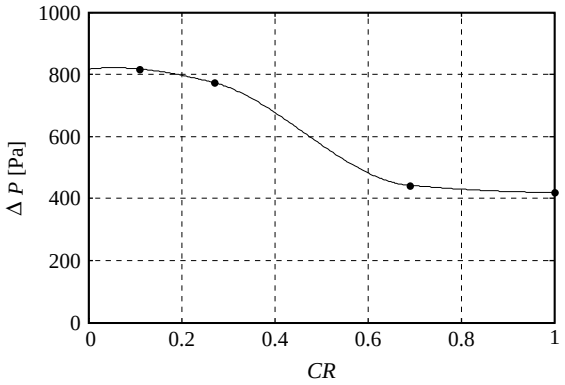

Figure 14. Pressure drop.

4. CONCLUSIONS

The effects of the contraction area ratio CR on the flow characteristics of the free jet issuing from an orifice nozzle were examined experimentally. The following conclusions were obtained.

(1) Significant dependency on CR on the large vortex structures of a submerged orifice water jet were observed in visualized images. The results implied that changing nozzle contraction ratio potentially controls the coherent vortex production.

(2) The centerline maximum velocity u_c/u_m can be expressed

$$u_c/u_m = 1.9CR^3 - 3.55CR^2 + 1.38CR + 1.53,$$

which has a maximum value of 1.7 at $CR = 0.27$.

Velocity vectors towards the centerline before the orifice nozzle exit caused by the contraction contributed to the increase in centerline velocity, which had a maximum of $CR = 0.27$.

(3) Jet and half widths demonstrated the dependency on *CR* at $x/d_o < 5$, while at $x/d_o > 5$, each width was the same for all *CR* cases. Thus, the contraction effects were found to be remarkable in the region near the nozzle exit. In addition, the entrainment flow rate increased with decreasing *CR* due to the thin shear layer at the nozzle exit.

NOMENCLATURE

A_i	Cross–sectional area of pipe
A_o	Nozzle exit area
b	Jet width at the location where the velocity ratio $u/u_c = 0.1$
$b_{1/2}$	Jet half width
CR	Contraction area ratio ($= A_0/A_i$)
d_i	Diameter of pipe
d_o	Diameter of nozzle exit
F_u	Flatness factor [$= (u'^4)/(u')^4$]
f	Frequency
f^*	Normalized frequency ($= f\, d_o/u_c$)
Q_x	Flow rate at the nozzle exit calculated by velocity profile
Q_0	Flow rate at the location x calculated by velocity profile
r	Spanwise distance from the center of nozzle
Re	Reynolds number ($= u_m\, d_o/v$)
St	Strouhal number ($= fd_o/u_m$)
S_u	Skewness factor [$= (u'^3)/(u')^3$]
u_c	Mean velocity along the centerline
u_m	Mean velocity at the nozzle exit
u'	Fluctuating velocity
x	Streamwise distance from the center of nozzle
Φ_u^*	Normalized power spectra density function

REFERENCES

1. Viskanta R, 1993, ‘‘Heat Transfer to Impinging Isothermal Gas and Flame Jets,’’ Exp. Thermal & Fluid Science, 6, pp. 111–134.
2. Antonia RA, Zhao Q, 2001, ‘‘Effect of initial conditions on a circular jet,’’ Exp. Fluids, 31, pp. 319–323.
3. Lee J, Lee SJ, 2000, ‘‘The effect of nozzle configuration on stagnation region heat transfer enhancement of axisymmetric jet impingement,’’ Int. J. Heat Mass Transfer, 43, pp. 3497–3509.
4. Quinn WR, 2006, ‘‘Upstream nozzle shaping effects on near field flow in round turbulent free jets,’’ European Journal of Mechanics B/ Fluid, 25, pp. 279–301.
5. Mi J, Nathan GJ, Nobes DS, 2001, ‘‘Mixing characteristics of axisymmetric free jets from contoured nozzle, an orifice plate and a pipe,’’ ASME J. Fluids Engineering, 123, pp. 878–883.
6. Gad-el-Hak M, Bandyopadhyay PR, 1994, ‘‘Reynolds number effects in wall-bounded turbulent flow,’’ App Mech Rev., 47, pp. 307–365.
7. Simpson RL, Chew YT, Shivaprased BG, 1981, ‘‘The structure of a separating turbulent boundary layer. 2. Higher-order turbulence results,’’ J. Fluid Mech., 113, pp.53–73.
8. Boguslawski L, Popiel Cz, 1979 ‘‘Flow structure of the free round turbulent jet in the initial region,’’ J. Fluid Mech., 90, pp. 531–539.